OPTICAL DIAGNOSTICS OF LATE INJECTION LOW-TEMPERATURE COMBUSTION IN A HEAVY DUTY DIESEL ENGINE

Thierry Lachaux, Mark P.B. Musculus
Sandia National Laboratories,
P.O. 969, MS9053
Livermore 94551, U.S.A.
e-mail: mpmuscu@sandia.gov

Satbir Singh
Powertrain Systems Research Lab
General Motors Research and Development
Warren, Michigan

Rolf D. Reitz
ERC, Department of Mechanical Engineering
The University of Wisconsin, Madison
1500 Engineering Drive, Madison, Wisconsin 53706, U.S.A.

ABSTRACT

A late injection, high exhaust-gas recirculation (EGR)-rate, low-temperature combustion strategy was investigated in a heavy-duty diesel engine using a suite of optical diagnostics: chemiluminescence for visualization of ignition and combustion, laser Mie scattering for liquid fuel imaging, planar laser-induced fluorescence (PLIF) for both OH and vapor-fuel imaging, and laser-induced incandescence (LII) for soot imaging.

Fuel is injected at top dead center when the in-cylinder gases are hot and dense. Consequently, the maximum liquid fuel penetration is 27 mm, which is short enough to avoid wall impingement. The cool flame starts 4.5 crank angle degrees (CAD) after the start of injection (ASI), midway between the injector and bowl-rim, and likely helps fuel to vaporize. Within a few CAD, the cool-flame combustion reaches the bowl-rim.

A large premixed combustion occurs near 9 CAD ASI, close to the bowl rim. Soot is visible shortly afterward, along the walls, typically between two adjacent jets. OH PLIF indicates that premixed combustion first occurs within the jet and then spreads along the bowl rim in a thin layer, surrounding soot pockets at the start of the mixing-controlled combustion phase near 17 CAD ASI.

During the mixing-controlled phase, soot is not fully oxidized and is still present near the bowl-rim late in the cycle. At the end of combustion near 27 CAD ASI, averaged PLIF images indicate two separate zones. OH PLIF appears near the bowl rim, while broadband PLIF persists late in the cycle near the injector. The most likely source of broadband PLIF is unburned fuel, which indicates that the near-injector region is a potential source of unburned hydrocarbons.

1. INTRODUCTION

Diesel engines are widely used throughout the world and satisfy a large customer demand, partly due to their higher energy efficiency compared to other engines. Pressure from the market for more energy-efficient engines and more stringent emission regulations have motivated improvements in diesel engine technology. Among regulated emissions are nitrogen oxides (NOx) and particulate matter (PM). NOx and PM are both affected by the fuel injection timing, pressure and rate of injection. Recent developments in high-pressure electronically-controlled common-rail injection systems give freedom to optimize the fuel injection schedule to reduce NOx and PM levels as much as possible.

These systems have also enabled new low-temperature combustion (LTC) strategies. LTC strategies can reduce the need for exhaust after-treatment by reducing engine out NOx and PM. To this end, they often use a large amount of exhaust gas recirculation (EGR) to lower the flame temperature and thereby reduce NOx production, and allow more time for air and fuel to premix to help decrease PM emissions [1-5]. Many LTC strategies have been demonstrated in diesel-type engines, including double injection such as Toyota's UNIBUS concept [6], early injection [7], or late injection such as Modulated Kinetics (MK) [1-3]. Unlike other strategies where an early injection yields a more premixed charge, the MK strategy uses a late injection occurring near or somewhat after top dead center (TDC) of the compression stroke. Due to the falling in-cylinder temperature and density after TDC, late fuel injection increases the ignition delay, which is the time between the start of injection (SOI) and the start of combustion. Extending the ignition delay enhances the pre-combustion air-fuel mixing, but the retarded combustion phasing may also decrease cycle efficiency. However, some have argued that with high swirl, heat transfer losses are reduced so that cycle efficiency can be maintained [1-3].

One significant drawback of MK combustion, and of LTC in general, is the increase of unburned hydrocarbons (UHC). UHC emissions, as well as soot and NOx formation, are strongly related to the physical and chemical processes occurring within the combustion chamber. For example, increasing swirl can help to reduce UHC emissions, but they

still remain higher than for conventional diesel combustion. Furthermore, many MK studies focused on small size direct injection (DI) diesel engines with large swirl numbers, reentrant piston bowls, and high engine speeds [1-5]. The in-cylinder mixing and combustion process in the quiescent chamber, large bore and medium speed-range of heavy-duty diesel engines may affect MK combustion processes very differently than in small-bore engines.

Using in-cylinder visualization, understanding of the important MK combustion processes can be improved and distilled into a conceptual model, along the lines of Dec's model for conventional diesel combustion [8]. Currently, little in-cylinder visualization data is available for the MK combustion strategy. The few examples include Kimura and coworkers [1-3], who showed that in-cylinder MK combustion is mainly non-sooty. Also, in a previous work [9], we presented combustion luminosity images of MK combustion in a large-bore engine. However, comprehensive visualizations of in-cylinder injection, mixing and combustion events of the MK strategy are not yet reported in the literature.

In the current study, in-cylinder combustion processes for an EGR-diluted, late-injection condition that is similar to MK combustion, but in a low-swirl heavy-duty diesel engine, are detailed using a set of optical diagnostics. The liquid fuel jet penetration is investigated using images of Mie scattering from liquid-fuel droplets. Two-stage ignition is visualized by chemiluminescence imaging. The liquid fuel visualization coupled with the chemiluminescence gives information on the temporal dwell between the injection and the ignition processes, which is an indicator of the potential for UHC emission [10]. Planar laser-induced fluorescence (PLIF) of the fuel molecules indicates the leading edge of the penetrating vapor-fuel jet. PLIF of OH marks the high-temperature combustion. Finally, soot is detected using soot luminosity and laser-induced incandescence (LII) techniques. OH and soot visualization provide a sequence of the main combustion heat release and the soot history.

2. EXPERIMENTAL SET UP AND DIAGNOSTICS

2.1 ENGINE AND INJECTOR

The engine is an optical single-cylinder diesel engine with the same bore and stroke as the production Cummins N-14 heavy-duty engine, 139.7 and 152.4 mm respectively. This configuration gives a displacement of 2.34 liters for the single cylinder engine. Table 1 provides engine characteristics, injector characteristics, and engine operating conditions. The engine configuration is further described in [7,8,11].

The quiescent chamber engine has a low swirl number (0.5). Because of modifications for optical access, the compression ratio is 11.2, compared to 16 for the production engine. To compensate, the intake pressure and temperature are elevated so that the thermodynamic state at TDC is typical of that for the production engine. To reduce the combustion temperature, the intake stream is diluted to 12.7% oxygen concentration (equivalent to approximately 60% EGR) by nitrogen addition. The engine was operated at a single, constant speed of 1200 rotations per minute (RPM) with a gross indicated mean effective pressure of 450 kPa, or roughly 25% of full load.

To provide optical access, the engine is equipped with an extended piston and a flat piston-crown window, as shown in Fig. 1 on the left side. A stationary mirror placed below the piston window provides a view of the combustion chamber to the camera/imaging system. Additional windows located around the top of the cylinder-wall provide cross-optical access for laser-based diagnostics. A portion of the piston bowl-wall was also fitted with an optical window that matched the contours of the bowl-rim, in-line with one of the cylinder-wall windows, as shown on the top-right in Fig. 1. This window allowed laser-sheet access into the combustion bowl of the piston, along the axis of one of the injector fuel-jets.

The non-production common-rail injector is electronically controlled and the rail pressure was 1600 bar. The mini-sac injector has 8 equally-spaced 0.196-mm diameter holes and an included angle of 152°. To avoid overheating, the optical engine was skip-fired once every ten cycles and an electric dynamometer maintained engine speed between fired cycles. Finally, in the operating conditions, listed in Table 1, the start of injection (SOI) value is the real, physical start of liquid-fuel injection, which is 3 CAD after the electronic firing signal.

2.2 OPTICAL DIAGNOSTICS

Two different laser systems were used in this study. First, an optical parametric oscillator, pumped by the third harmonic of a Nd:YAG laser at 355 nm, generated 10-Hz, 10-ns pulsed laser radiation near 568 nm, which was frequency-doubled to near 284 nm with 17 mJ per pulse for the fluorescence diagnostics (described below). Second, a 10-Hz frequency-doubled Nd:YAG laser generated 10-ns pulses at 532 nm with 35 mJ per pulse for the other two laser diagnostics. Both beams were converted into thin (less than 1 mm thick) sheets using a combination of cylindrical and spherical lenses. As shown in Fig. 1, the two sheets were overlapped and directed into the cylinder at a slope of 14° from horizontal, which is parallel to the axis of the fuel jet that was in-line with the cylinder-wall and piston bowl-rim windows. After being clipped by the window aperture, the sheet was about 35 mm wide inside the combustion chamber.

The combustion chamber was visualized through the piston crown window using two UV-sensitive, gated, intensified CCD video cameras. To achieve simultaneous imaging, the signals were chromatically separated by a 450-nm cut-off dichroic beamsplitter, which reflected ultraviolet (UV) light and transmitted visible light (see Fig. 1). The camera receiving long-wavelength (visible) light was equipped with a Nikkor 105-mm f/2.5, glass lens. The camera receiving short-wavelength (UV) light was equipped with a UV-Nikkor 105-mm f/4.5 lens. In addition, a filter pack appropriate for the diagnostic of interest was placed in front of the lenses for each camera, as described in the following paragraphs.

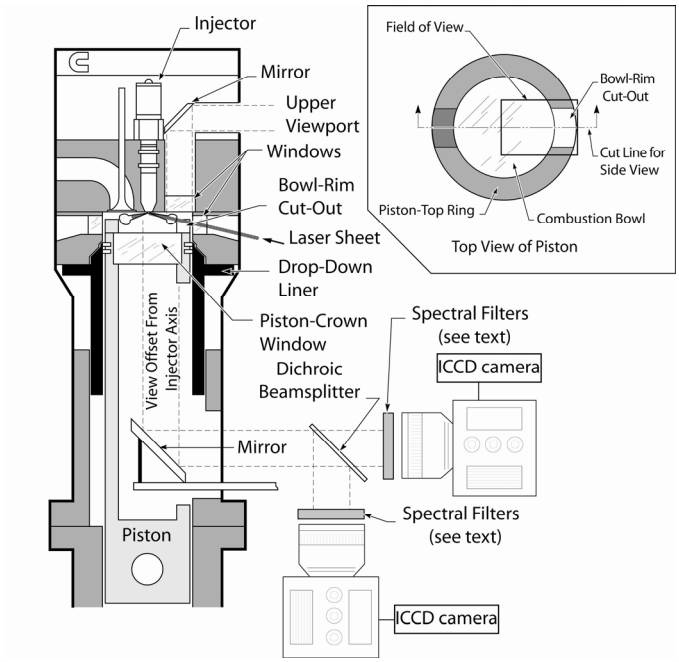

FIGURE 1. Engine cross-section schematic and optical diagnostics set-up and field of view from the piston window (inset).

The liquid-phase diesel fuel was imaged by collecting the Mie-scattered light from liquid droplets (liquid Mie scattering, or LMS) illuminated by the 532-nm laser sheet and using a 532-nm band pass filter (BPF). The 532-nm laser beam also induces weak elastic Rayleigh scattering from the vapor phase fuel, but the Mie scattered light is many orders of magnitude stronger than the Rayleigh scattered light [12]. As a result, only liquid-fuel Mie-scattering is discernable within the dynamic range of the camera. A neutral density filter attenuated strong elastic scatter to avoid damaging the intensified CCD camera and to ensure that it operated in its linear regime. The camera electronic gate was set to 120 ns. The technique is described in more detail in [13].

Ignition chemiluminescence and soot luminosity are line-of-sight averaged diagnostics. To avoid excessive smearing due to fluid motion, the camera gatewidth was set to 70 microseconds, which is equal to one-half CAD at 1200 RPM. The chemiluminescence emission is due to many species including CH, C_2 and formaldehyde (H_2CO) [14-16], but other radicals are present as well. The emission is relatively weak, so to maximize signal strength, no spectral filters were used and thus no specific species were tracked. The other much stronger source of photonic emission is due to naturally occurring soot incandescence. Soot typically forms after the premixed-combustion phase, and its emission is many orders of magnitude stronger than chemiluminescence [16].

Soot LII was excited by the Nd:YAG laser second harmonic at 532 nm. Three filters, a 480-580 notch filter, a 380-450 BPF and a 330-620 BPF in front of the camera isolated the LII signal from elastic scatter. The camera gate was set to 100 ns. This LII filtering scheme is essentially the same as that described in [11,17,18].

TABLE 1: Engine specifications, injector specifications and operating conditions

Engine base type	Single cylinder 4-stroke Cummins N-14, DI Diesel
Number of intake valves	2
Number of exhaust valves	1*
Combustion chamber	Quiescent, direct injection
Swirl ratio	0.5
Bore × Stroke	139.7 mm × 152.4 mm
Bowl width, depth	97.8 mm, 15.5 mm
Displacement	2.34 liters
Connecting rod length	304.8 cm
Geometric compression ratio	11.2:1
Simulated compression ratio	16:1
Fuel injector type	Common rail , pilot valve actuated
Cup (tip) type	Mini sac
Number of holes	8, equally spaced
Spray pattern included angle	152°
Rail pressure	1600 bar
Nozzle orifice diameter	0.196 mm
Nozzle orifice L/D	5
SOI	360 CAD (TDC)
Mass injected per cycle	56 mg
DOI	9 CAD
Intake Temperature	70°C
Intake Pressure	202 kPa
Intake Oxygen Concentration	12.7% (~60% EGR)
Temperature at TDC	840 K
Density at TDC	22.7 kg/m^3
Engine Rotational Speed	1200 rpm

*In this optically accessible diesel engine, one of the two exhaust valves of the production cylinder head was replaced by a window and periscope.

Finally, a single UV fluorescence technique yielded information about either OH or fuel distributions, depending on the sensitivity of the fluorescence signal to the laser wavelength. First, OH fluorescence was excited at 284.01 nm and fluorescence was observed near 310 nm. A set of three filters (310 nm unblocked narrow BPF, 310 nm blocked BPF with 90 nm FWMH, and color glass SWG305) were placed in front of the camera to isolate OH-PLIF from elastically scattered light.

OH, however, displays a unique, well-defined fine-scale ro-vibrational structure in its fluorescence excitation spectrum. As a result, the OH fluorescence decreases drastically as the laser wavelength is tuned off any of the narrow excitation lines. By contrast, interfering fluorescence from other species, such as polycyclic aromatic hydrocarbon (PAH) soot precursors or fuel aromatics, is insensitive to small changes in the excitation wavelength. Therefore, to identify the extent and spatial location of the interference, the OH-PLIF images

were taken at two different wavelengths: on-line, near 284.01 nm, and off-line, near 283.90 nm. A locally stronger on-line signal indicates the presence of OH. More details, including the filter selection criteria, can be found in [19].

The second fluorescence technique applies when the on-line and off-line fluorescence signal strengths are similar. If no fine-scale absorption structure is apparent, then the fluorescence is from broadband sources (*i.e.*, BB-PLIF). The laser wavelength and filters for the BB-PLIF technique are the same as those for the OH-PLIF technique. Early in the cycle, before significant chemical reactions, the most likely source of BB-PLIF is fluorescing components of the liquid- and vapor-phase fuel. Later in combustion, other species, such as PAH soot precursors and other combustion intermediates may also contribute to the BB-PLIF. Additional details can be found in [20].

Finally, due to repetition-rate limitations of the lasers (10 Hz), only one image could be acquired for each engine cycle. For each crank angle, images were acquired in sets of 12, from 12 different cycles. Either a representative instantaneous image was then selected from each set, or an ensemble-averaged image was extracted. Depending on the analysis required, these selected images were compiled into temporal sequences.

3. COMBUSTION AND INJECTION EVENTS

3.1. APPARENT HEAT RELEASE RATE AND COMBUSTION PHASES

The apparent heat release rate (AHRR) was determined from the cylinder pressure, using an air-standard first-law analysis [21]. Prior to calculating the AHRR, the pressure data were smoothed using a Fourier-series low-pass filter with a Gaussian roll-off function having a transmission of 100 % from 0 to 800 Hz and dropping to 1 % at 3360 Hz. These cut-off frequencies were selected to remove acoustic ringing caused by combustion pressure oscillations in the cylinder pressure data while retaining the general features of the AHRR. Due to this filtering, the peak of the premixed burn spike in the filtered AHRR was reduced by about 14 %, while its width was increased by a factor of 1.2. However, the apparent energy release (area under the AHRR curve) during the premixed burn was virtually unchanged by this filtering technique. The filtering technique does not significantly alter the critical features of AHRR such as the time of transition for different phases of combustion, including the ignition delay.

The injection rate signal and AHRR are plotted on Fig. 2. The injection rate was derived from the spray momentum, measured at atmospheric pressure in a closed vessel, as described in [7,22]. In the engine, the fuel is injected at TDC where in-cylinder gases reach maximum compression and thereby promote fuel vaporization. The temperature at the start of the injection event (TDC), estimated from a polytropic law, is 840 K. At the start of injection (360 CAD), the AHRR starts to decrease, due to cooling by the vaporizing fuel. After vaporization, the AHRR plotted in Fig. 2 exhibits three distinct combustion phases. As discussed in the next section, the precise beginning of the first phase depends on its definition, but using the first zero-crossing of the AHRR in Fig. 2, the first "cool-flame" phase starts at 366 CAD. The first phase ends between 369 and 370 CAD, overlapping with the beginning of the second phase, premixed-combustion. The premixed-combustion phase lies between 370 and 377 CAD. Finally, the third phase, mixing-controlled combustion, lies between 377 and 387 CAD.

A previous study [10] related these three combustion **phases** to typical two-**stage** chemistry. The low-temperature cool-flame and slow oxidation processes start and end during the first phase. They release a small amount of the total heat and characterize the first-stage chemistry; the maximum AHRR of the cool-flame phase is about 12 % of the peak premixed-combustion AHRR. The second-stage chemistry is involved in both the premixed- and mixing-controlled-combustion phases, where the rest of the fuel chemical energy is released.

As for the other LTC strategies, the ignition delay for MK combustion is typically longer than the injection duration so that injection and combustion do not overlap. In these experiments, the cool-flame phase and the injection do overlap slightly, but the premixed-combustion phase does not overlap at all with the injection. Furthermore, the injection rate is rapidly decreasing during the overlap with the cool-flame phase, so significant premixing still occurs before premixed combustion, as will be seen in the next sections.

3.2. INJECTION AND COOL-FLAME PHASE

Superposition of virtually simultaneous images of LMS and BB-PLIF (fuel) are presented in Fig. 3. A comparison of on-line and off-line signals in the BB-PLIF images (as described in section 2.2 for OH-PLIF), not shown here, indicates that there is no OH-PLIF and nearly all of the BB-PLIF is therefore due to fuel components. The 10-ns laser pulses for LMS and BB-PLIF were separated by 1 microsecond to avoid any interference in the signals for the two diagnostics. The images are ensemble-averaged over 12 cycles. The effective camera gain for each diagnostic is displayed at the bottom of each image, and the relative gain is valid only for a given

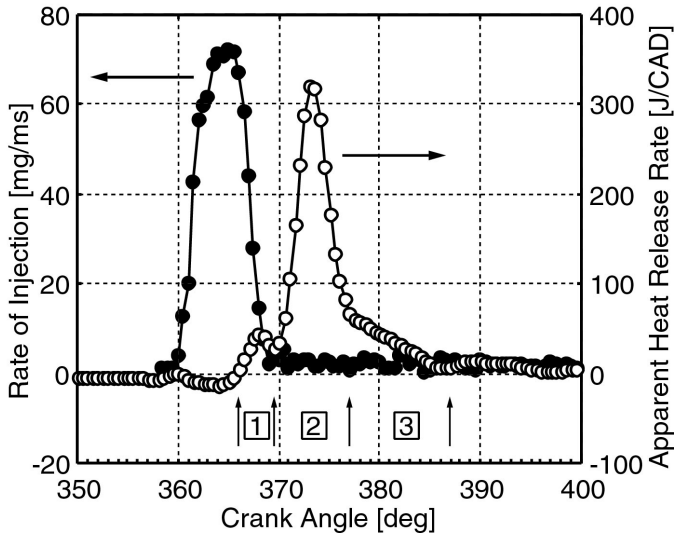

FIGURE 2. Mass rate of injection and apparent heat release rate. The boxed numbers 1, 2 and 3 represent the cool-flame phase, the premixed-combustion phase, and the mixing-controlled phase, respectively.

camera. That is, the gain for the BB-PLIF camera is different from the gain for the LMS camera. The laser sheet propagates from right to left. The field of view is limited by the bowl rim on the right side, and the injector is visible on the left side, indicated by a white dot. The false blue color displays the LMS signal corresponding to the liquid phase of the jet, while the false green color represents the BB-PLIF signal.

The BB-PLIF signal is due to emission from both liquid and vapor fuel, which cannot be distinguished from each other using BB-PLIF images alone. However, comparison with the LMS images, which show only liquid-phase fuel, can provide guidance for interpreting the BB-PLIF images. For example, considering the horizontal jet (3 o'clock position) at 364 CAD and later, the UV beam (BB-PLIF) at 284 nm crosses first the leading edge of the jet and is strongly absorbed by fuel vapor, so that very little laser light reaches the liquid fuel spray. (Some attenuation is also apparent in the 362 CAD image.) Furthermore, the LMS image at 364 CAD shows that that liquid fuel in the horizontal jet (blue) is entirely upstream of the BB-PLIF signal (green). Consequently, for 364 CAD and later, only the vapor-phase fuel appears in the BB-PLIF images for the horizontal jet. The absorption by the leading edge of the horizontal jet is also responsible for the lack of BB-PLIF signal in the upstream region of the jet at 364 CAD and later.

The initial liquid jet is detected at 360 CAD in Fig. 3. At 361 CAD, some vapor-phase fuel is first visible in the BB-PLIF image outside of the periphery of the liquid-phase fuel in the LMS image. That is, fluorescence in the green BB-PLIF image is from both vapor and liquid fuel, but the liquid-fuel location is clearly identified by the overlapping blue LMS image. Therefore, the purely green color on the periphery of the 361 CAD image (without overlapping of blue color from LMS) indicates vapor fuel only. At 362 CAD, the blue liquid phase penetrates farther, and the green vapor phase expands at the leading edge of the horizontal jet. As aforementioned, the 284-nm light sheet is absorbed by vapor fuel located downstream at the leading edge of the jet, so the fuel closer to the injector tip is not illuminated in the BB-PLIF image. However, the UV laser sheet can reach the sides of the adjacent jets at the 1 o'clock and 5 o'clock positions. These jets show some vapor fuel fluorescence (green) closer to the injector, in addition to the liquid fluorescence (green and blue overlap). Therefore, the vapor fuel surrounds the entire liquid-phase spray.

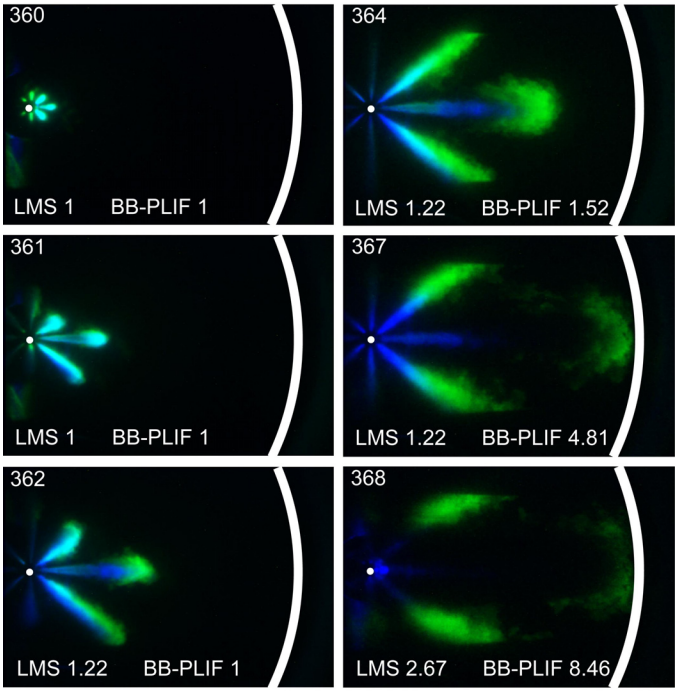

FIGURE 3: Liquid-phase (LMS, blue) and vapor-phase (BB-PLIF, green) fuel. The crankshaft angle is displayed on the top left corner and the LMS and BB-PLIF gains are on the bottom of each image. The small white dot marks the injector location and the thick white line indicates the location of bowl-rim, 50 mm from the injector.

At 364 CAD, the vapor-fuel region located at the head of the jet (green) penetrates downstream of the liquid fuel. The shape and geometry of the liquid spray is typical of conventional diesel sprays, which also have short penetration [8,23]. Figure 4 shows the evolution of the liquid length of the horizontal jet, defined as the farthest downstream location where the LMS image intensity is higher than 10% of the difference between the lowest (background) and highest (in the liquid jet) intensity of the image. The signal intensity has been found nearly constant along the background level. The intensity gradient in the LMS images at the tip of the liquid spray is steep, so intensity thresholding works well to measure the liquid penetration. A 10 % threshold has been found to provide reliable liquid length measurements [24].

Figure 4 shows that from 363 to 366 CAD, the liquid length reaches its maximum value of 26 to 27 mm and remains approximately constant for about 3 CAD. This short-injection liquid length can be compared to predictions of Siebers' scaling law for liquid penetration of steady diesel fuel sprays [25]. In Siebers' spray model for steady jets, the vaporization rate in the downstream part of the jet counterbalances the fuel injection rate. Among many factors, hole diameter, fuel characteristics (volatility, fuel temperature)

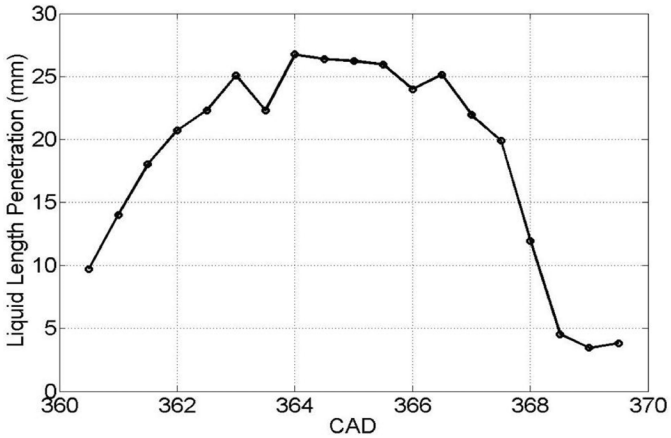

FIGURE 4. Liquid length extracted from the liquid Mie scattering (LMS) instantaneous images.

and thermodynamic factors (ambient density and temperature) affect the liquid length. In our single cylinder engine with injection near TDC, the ambient density and temperature are approximately 22.7 kg/m^3 and 840 K. For these conditions, the scaling law for steady jets predicts a liquid length of about 35 mm, which is somewhat greater than the 26 to 27 mm maximum liquid penetration of the jet in the current study (see Fig. 4). Differences in the orifice coefficients or the spray spreading angle may account for some of the difference, as well as the short injection duration of the current study, for which the full, steady liquid length may not be established.

The large distance from the injector to the bowl rim in heavy-duty diesel engines and the high-density, hot in-cylinder environment near TDC help to prevent impingement of liquid fuel on the combustion chamber walls. Impingement sometimes occurs with early-injection LTC strategies [13], and avoiding impingement might prevent additional soot and UHC emissions resulting from wall-wetting. Hotta et al. [26] note that in a small indirect injection diesel engine at medium to high-load conditions, wall impingement by the liquid-jet creates a locally rich-fuel mixture that causes increased exhaust soot emission. Tsurushima et al. [27] confirm that liquid wall impingement in a small direct injection diesel engine yields UHC emissions. However, for a large bore DI diesel engine, Fig. 4 shows that the liquid fuel penetration is too short to cause wall impingement of the liquid fuel for these near-TDC injection conditions.

Figure 5 displays a sequence of chemiluminescence images. For each CAD, 12 images are ensemble averaged. Chemiluminescence identifies spatial and temporal locations of ignition. The initial signal from chemiluminescence in Fig. 5 is very low relative to later in the cycle, as indicated by the high camera gain (displayed at the bottom left corner). The beginning of the first combustion stage is detected at 364.5 CAD, half-way between the injector and the bowl rim. This chemiluminescence occurs 1.5 CAD earlier than the first zero-crossing of the AHRR in Fig. 2. The small amount of heat released during the first ignition stage is likely not enough to significantly affect the pressure trace, so it does not increase the AHRR significantly. Moreover, any small increase of pressure which could occur during the beginning of this first stage ignition is likely offset by the decrease of pressure from liquid vaporization. Consequently, the actual the start of combustion is somewhat ambiguous, because chemiluminescence emission begins 1.5 CAD earlier than the first zero-crossing of the AHRR.

At 367 CAD, referring back to Figs. 3 and 4, the liquid length begins to decrease, while the leading edge of the vapor fuel of the horizontal jet reaches the bowl rim. Again, attenuation by the head of the horizontal jet does not allow the laser to illuminate fuel in the upstream region of the horizontal jet, so no information about upstream vapor fuel is available. However, the adjacent jets, which are illuminated from the side, show that vapor fuel does extend back toward the injector. The region very near the injector for all of the jets is not illuminated due to attenuation by the wide head of the horizontal jet, so no information about vapor fuel very near the injector can be discerned from the later images in Fig. 3.

At 367.5 CAD, the chemiluminescence in Fig. 5 indicates that the combustion zone reaches the bowl rim, and the jets are clearly flattening against the bowl rim. At 367.5 CAD, the top of the piston is close to the firedeck (around 5 mm), thus most of combustion likely occurs within the piston bowl. Combustion is still in the cool-flame phase (Fig. 2), though the camera gain is reduced by an order of magnitude from the 367 CAD image because of increased chemiluminescence intensity.

The physical end of injection occurs near 368 CAD (see Fig. 2). Referring back to the 368 CAD image in Fig. 3, some liquid fuel spray remains, but with a much shorter length and weaker LMS signal. The heat released by the combustion, including both first-stage and maybe some second-stage reactions, occurs at the same time and likely aids the evaporation process.

At 369 CAD in Fig. 5, the reaction zone starts to spread circumferentially along the bowl rim as combustion transitions to the premixed phase.

3.3 PREMIXED PHASE

Near the bowl-rim at 369.5 CAD in Fig. 5, the downstream part of the jet becomes much brighter. Eventually it merges with adjacent jets and forms a large ring along the bowl wall at 372.5 CAD, with much brighter emission as indicated by the decreasing gain. The strong natural luminosity at 372.5 CAD originates from soot, as will be confirmed later in this section by the LII images of Fig. 7. Note that the ring shape appears because of the averaged pictures. Indeed, instantaneous

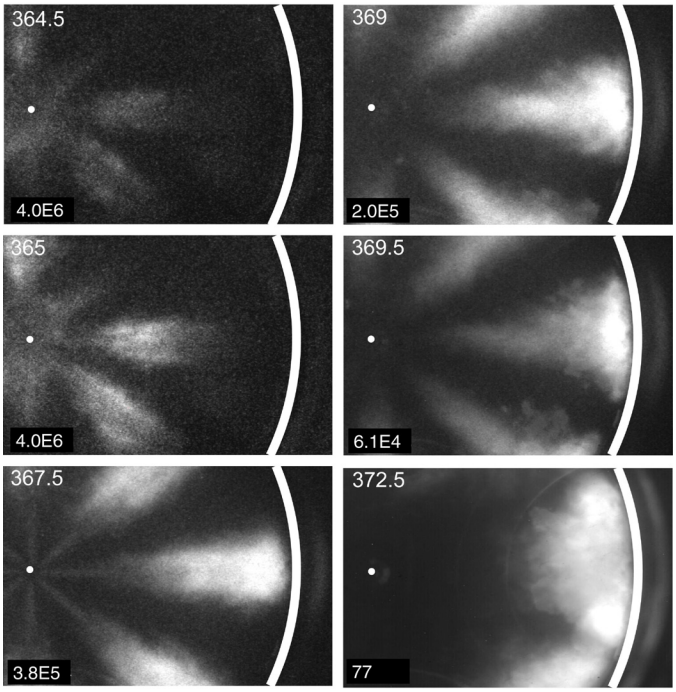

FIGURE 5. Chemiluminescence averaged pictures. The crank angle is displayed on the top left corner while the relative gain is displayed at the bottom left corner. The small white dot marks the injector location and the thick white line indicates the location of bowl-rim, 50 mm from the injector.

images in Fig. 7 show soot in pockets between two adjacent jets, near the bowl-rim.

The peak AHRR also occurs near 372.5 CAD (Fig. 2), where soot luminosity first becomes strong. In a small-bore engine with low EGR, Miles *et al.* observed soot appearing in the jet similar to conventional diesel injection strategies [4]. For high EGR conditions, with 15% intake O_2 (comparable to the 12.7% level in these experiments), soot formation was delayed and a distinct jet structure was no longer apparent [4]. In our experiment, injection occurring close to TDC leads to a shorter ignition delay, and with very little swirl, the jet structure remains at the onset of soot formation.

Figure 6a presents the local natural luminosity intensity (both chemiluminescence and soot incandescence) for various CAD, computed with averaged images, along the centerline of the jet from the bowl rim to roughly 8 mm downstream of the injector tip. This intensity is corrected for the varying camera gains. During the combustion sequence, the most intense luminous region moves from the upstream to downstream. The intensity from the cool flame (364.5 to 365 CAD) is lower by a factor of 5 to 6 orders of magnitude than the intensity from soot (373 CAD). In addition, the straight lines on the graph indicate an approximately exponential evolution in time and at least one order of magnitude difference in intensity along the jet centerline.

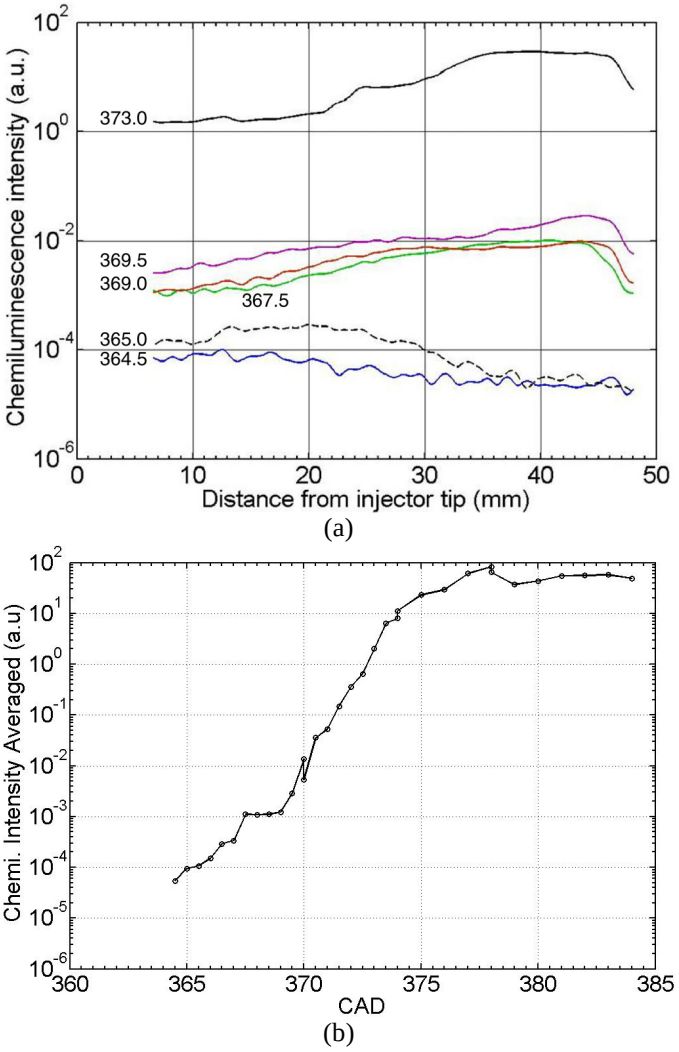

FIGURE 6. Natural luminosity intensity, plotted (a) along the jet centerline, and (b) averaged along the centerline.

Figure 6b presents the combustion natural luminosity intensity described previously but averaged along the jet centerline, versus CAD. The intensity increases by seven orders of magnitude, roughly exponentially with time between 366 CAD where the cool flame occurs and 374 CAD at the AHRR peak. Thereafter, the emission reaches an asymptote corresponding to the strong soot emission. As an alternative method, the combustion intensity was also averaged over a 45-degree sector from the injector tip to the bowl rim. The results are not reported here, but the results are essentially the same as Fig. 6b.

Figure 7 shows instantaneous, simultaneous false-color images of LII (red) and OH PLIF (green). Due to the cycle-to-cycle variation, images are selected as the best representatives at each CAD. First, considering the red LII images, soot is mostly present in large pockets near the bowl rim (downstream in the jet) in both the lower- and the upper-right corners of the laser sheet, as visible at 376 CAD for example. The soot LII in the upper-right corner generally appears weaker because that soot is carried out of the laser sheet by the weak swirl. Recall that the rapidly increasing brightness in the natural luminosity images in Fig. 5 suggested that soot starts to form close to the bowl rim. We reported similar soot locations in earlier experiments at the same operating condition in this engine [20]. Also, in [30], soot appeared downstream, between adjacent jets in a different DI heavy-duty diesel engine. The interaction at the bowl wall between adjacent jets could form a rich fuel zone, therefore creating soot. It is shown in [30] that an oxygenated fuel helps to decrease the local equivalence ratio and thereby decreases soot formation at where the jets interact along the bowl wall.

Considering the green OH-PLIF images in Fig. 7, the OH fluorescence, which first appears near 373 CAD, must be discriminated from BB-PLIF, which is also present. Unfortunately, instantaneous on-line and off-line images cannot be acquired at the same time. Rather, the general behavior of on-line OH-PLIF must be compared to the general behavior of off-line OH-PLIF. Figure 8 displays four ensemble-averaged images of OH-PLIF taken on-line (red) superimposed with images taken off-line (green). The pure red color indicates OH fluorescence, because OH fluoresces at the on-line wave length and not at the off-line wave length. The pure green color indicates that a compound which is not OH fluoresces at the off-line wavelength, and very little OH-PLIF is present. A yellow color indicates that the on-line and off-line signal overlap. In other words, the yellow color indicates that something is fluorescing at both on-line and off-line (not OH) wavelengths, though some OH may be present too. The black color indicates either no fluorescence sources are present, or that the laser light is absorbed and cannot reach the area.

At 373 CAD, OH (red and perhaps yellow) is mainly located between midway from the injector tip to the bowl-rim and the

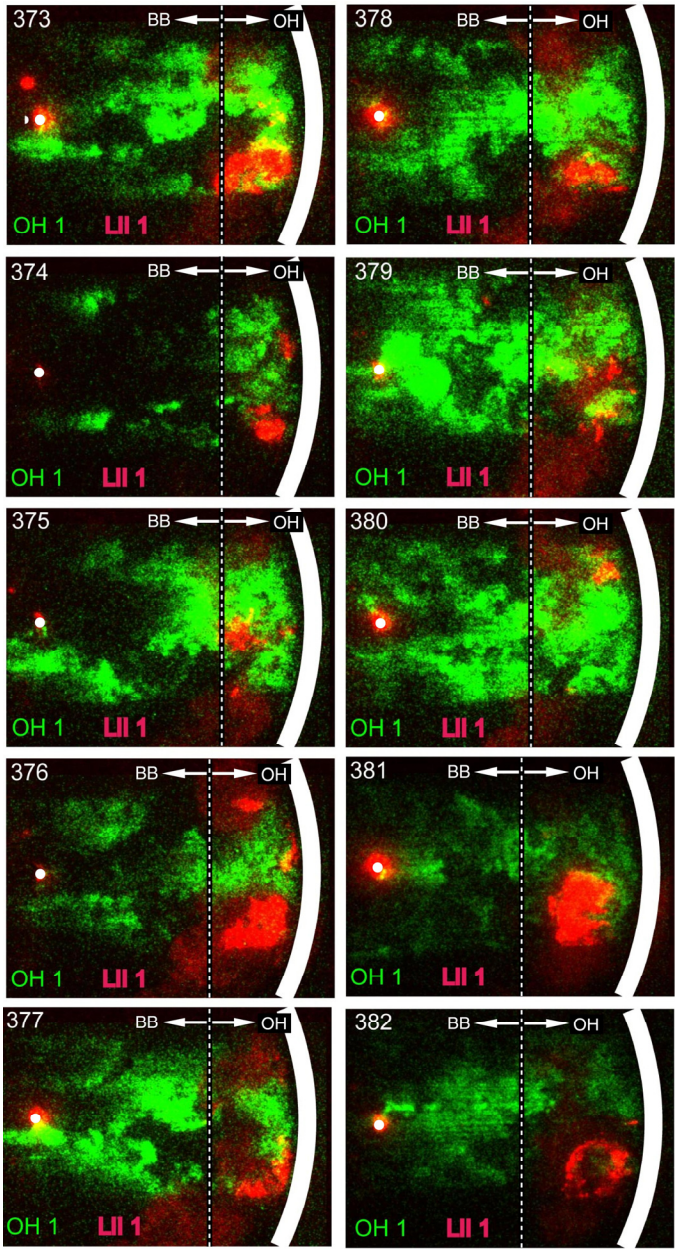

FIGURE 7. Instantaneous images from fuel and OH fluorescence (green) and laser induced incandescence (red). The crank angle is displayed at the top left corner of the picture while the relative gains are displayed at the bottom. The small white dot marks the injector location and the thick white line indicates the location of bowl-rim, 50 mm from the injector. The vertical dashed line indicates the approximate separation of fluorescence from OH, on the right, and broadband sources (*e.g.*, fuel), on the left.

bowl-rim. The OH becomes more dominant close to the bowl rim at 374 CAD and at 375 CAD, where the red color covers a larger area. Similarly to Fig. 7, a dark zone is located between injector tip and midway between the injector tip and the bowl-rim at 373 and 374 CAD. As explained earlier, this dark zone is due to the laser-sheet attenuation. From 375 to 380 CAD, most of the OH is located near the bowl rim. Therefore, the fluorescence observed on the right-hand side of the vertical

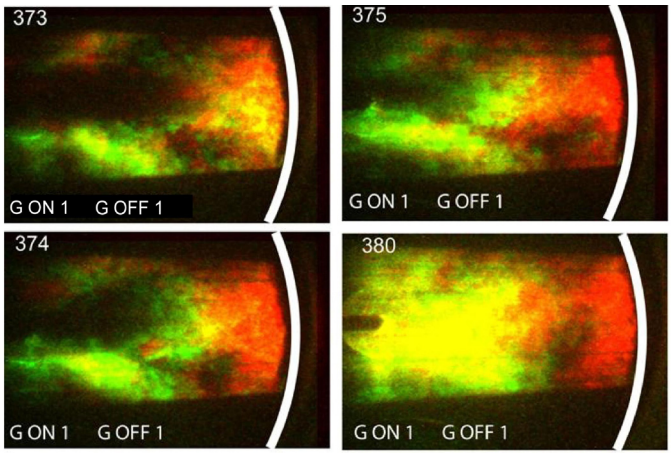

FIGURE 8. On-line (red) and off-line (green) ensemble averaged OH-PLIF images. The crank angle is displayed on the top left corner while the relative gains are displayed on the bottom. The small white dot marks the injector location and the thick white line indicates the location of bowl-rim, 50 mm from the injector.

dashed line in Fig. 7, between the two soot pockets from 378 to 380 CAD, is expected to be OH, based on the strong contrast between on-line and off-line averaged images in Fig. 8. The fluorescence signal near the injector, on the left-hand side of the dashed vertical line, most likely fuel fluorescence. Certainly, it is some product of incomplete combustion, since complete combustion products (H_2O and CO_2) do not fluoresce at these wavelengths. Also, formaldehyde chemiluminescence attributed to cool-flame reactions has been observed upstream of OH chemiluminescence [28], similar to the proximity of cool flame chemiluminescence (Fig. 5 at 365 CAD) and OH-PLIF (Figs. 7 and 8 near 373 CAD) of the current study.

Figure 9 displays selected representative, instantaneous, superimposed pictures of OH and natural luminosity. Recall that natural luminosity is integrated along the line of sight, while the OH-PLIF originates from the laser sheet only. Comparison with Fig. 7 confirms that the red-colored pockets near the bowl rim are certainly natural luminosity from soot, with strong OH-PLIF generally farther upstream. Similar behavior was reported for an early-injection LTC condition in the same engine, with broad distributions of OH downstream and pockets of soot at the head of the jet [20]. Also, in a constant-volume combustion vessel under similar conditions, with kernels of soot formed downstream of OH chemiluminescence [28].

3.4 MIXING-CONTROLLED PHASE

From 378 through 383 CAD in Figs. 7 and 9, fuel and OH fluorescence becomes more broadly distributed during the mixing-controlled phase. In Fig. 8 (on-line/off-line averaged images), OH typically appears from the bowl rim to half way to the injector tip for 375 to 380 CAD. The complementary region, from the injector through half-way to the bowl rim, has a strong off-line signal. Once again, the most likely source of the off-line signal is unburned fuel. At 383 CAD, the AHRR

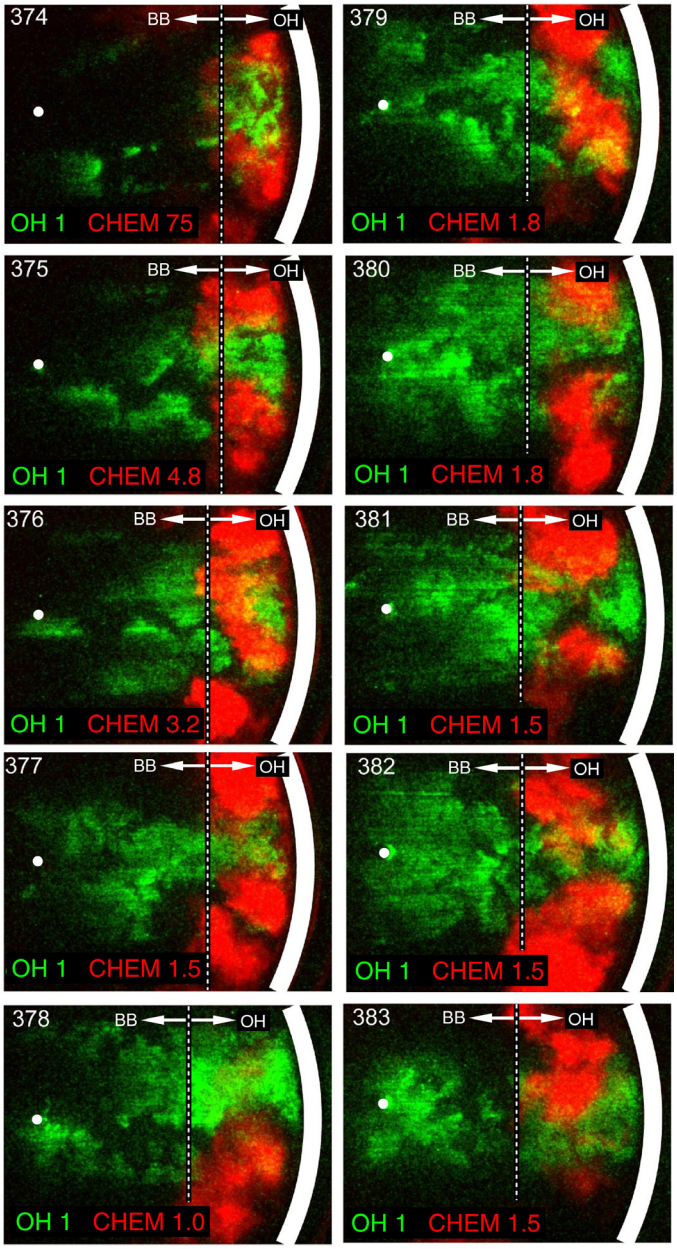

FIGURE 9. Instantaneous images of simultaneous OH fluorescence (green) and chemiluminescence and/or soot luminosity (red). Annotation is same as for Fig. 7

is very low and the fuel likely remaining near the injector represents a potential source of unburned hydrocarbons.

Large soot pockets remain late in the cycle in Figs. 7 and 9. The AHRR (Fig. 2) indicates that combustion is almost completed by 383 CAD, so much of the soot may survive into the exhaust. In [18], the authors noted that with a retarded injection and N_2 dilution as a surrogate for EGR, soot increased significantly. They saw more soot LII with less OH-PLIF than in the normal timing. Miles et al. [4] observed that soot was not concentrated near the bowl rim, but rather it was more dispersed throughout the combustion chamber. The more compact soot pockets of the current study could be due to the lower swirl than used in [4].

3.5 COMPARISON TO CONVENTIONAL DIESEL

Compared to conventional diesel combustion, the LTC strategy implemented here uses a higher rate of EGR, which increases the specific heat capacity, which in turn dramatically decreases combustion temperature. Hasegawa et al. [31] used Chemkin / Senkin [32,33] in shock tube calculations to test separately the heat capacity and oxygen concentration influence on ignition delay. Increasing heat capacity and/or decreasing oxygen concentration both delayed the start of combustion. They also showed that the main heat release is delayed because of a slower reaction rate of H_2CO, as also presented in [10].

In a conventional diesel combustion strategy, combustion and injection typically overlap temporally. A large fraction of conventional diesel combustion occurs in the mixing-controlled phase with locally rich mixtures and diffusion combustion [21]. The stoichiometric diffusion flame produces locally high-temperature regions favorable to NOx production. In LTC, due to the longer ignition delay, combustion starts after the end of injection and gives more time for fuel and air to premix. A large fraction of LTC combustion occurs in the premixed combustion phase with a lower flame temperature because of EGR dilution. Furthermore, the mixing controlled combustion phase duration is reduced [34]. Both effects may help to decrease the NOx emissions.

Pickett *et al.* [35] analyzed soot formation using Senkin [33] and a two-stage Lagrangian model simulation. Oxygen concentration was shown to affect soot formation processes. LTC strategies with lower intake oxygen concentrations have longer residence times for soot precursor formation in locally fuel-rich mixtures. However, lower temperatures decrease the production rate of soot precursors. As a result of these two contradictory effects, soot precursors first increase with decreasing oxygen concentration (typically down to 15% O_2) then quickly decrease, reaching near-zero levels around 8% O_2 [35]. These results were later verified experimentally by Idicheria and Pickett [36]. In the current study, the reduced oxygen concentration and lower combustion temperatures act to reduce the soot formation relative to conventional diesel combustion.

4. SUMMARY AND CONCLUSIONS

A low-temperature combustion (LTC) strategy with late injection and high EGR was visualized within the combustion chamber in a heavy-duty diesel engine using a set of optical diagnostics: Mie scattering to investigate liquid-fuel droplets, chemiluminescence imaging to visualize ignition and combustion, BB-PLIF and OH-PLIF to indicate the penetrating vapor-fuel jet and the combusting regions, and natural luminosity and LII to detect soot. Three distinct combustion phases can be extracted from the AHRR for this LTC condition: cool-flame (first phase), premixed combustion (second phase) and mixing-controlled combustion (third phase). Many features of late-injection LTC combustion are similar to those previously reported for early-injection LTC [20], as summarized in the following paragraphs.

Injection starts at top dead center. The liquid jet is relatively short, similar to that in conventional diesel combustion, and with no wall impingement by liquid fuel. From an engineering point of view, the results show that liquid wall-impingement is avoided because of the hot, dense in-cylinder conditions at this injection timing. The vapor phase expands quickly after SOI, especially in the leading edge region of the jet.

The cool-flame reactions start before the end of injection, but the main premixed combustion phase occurs after the end of injection. Cool-flame chemiluminescence is first detected half-way between the injector tip and bowl-rim. A few CAD later, the chemiluminescence spreads along the bowl-rim as the premixed-combustion phase commences and chemiluminescence intensity increases dramatically.

Soot starts to form along the piston bowl-wall typically between two adjacent jets. OH radical imaging indicates that premixed combustion first occurs downstream in the jet and then spreads along the bowl rim.

During the mixing controlled phase, OH is detected in the region halfway between the injector and the bowl rim, while unburned fuel likely remains near the injector. This lingering fuel is a potential source of unburned hydrocarbon emissions. Later in the cycle, soot is not completely oxidized in the low-swirl engine of this study, likely contributing to exhaust PM emissions.

5. ACKNOWLEDGMENTS

The experiments were performed at the Combustion Research Facility, Sandia National Laboratories, Livermore, CA. Sandia is a multiprogram laboratory operated by Sandia Corportation, a Lockheed Martin Company, for the United States Department of Energy's (DOE) National Nuclear Security Administration under contract DE-AC04-94AL85000. The United States Government retains and the publisher, by accepting the article for publication, acknowledges that the United States Government retains a non-exclusive, paid-up, irrevocable, world-wide license to publish or reproduce the published form of this manuscript, or allow others to do so, for United States Government purposes. Financial support was provided by DOE's Office of FreedomCAR and Vehicle Technologies, managed by Kevin Stork and Gurpreet Singh. The authors also thank David Cicone of Sandia National Laboratories for his assistance in maintaining the optical-access research engine used in these experiments.

6. ACRONYMS AND ABBREVIATIONS

AHRR:	Apparent Heat Release Rate
ASI:	After the Start of Injection
BB-PLIF:	Broadband Planar Laser-Induced Fluorescence
BPF:	Bandpass Filter
CAD:	Crank Angle Degrees
DI:	Direct Injection
EGR:	Exhaust Gas Recirculation
LII:	Laser-Induced Incandescence
LMS:	Liquid Mie-Scattering
LTC:	Low-Temperature Combustion
MK:	Modulated Kinetics Combustion
NOx:	Nitrogen Oxides (NO and NO_2)
PAH:	Polycyclic Aromatic Hydrocarbons
PLIF:	Planar Laser-Induced Fluorescence
PM:	Particulate Matter
RPM:	Rotations Per Minute
SOI:	Start of Injection
TDC:	Top Dead Center
UHC:	Unburned Hydrocarbons
UV:	Ultraviolet

7. REFERENCES

[1] Kimura, S., Aoki, O., Ogawa, H., Murakana, S., Enomoto, Y., 1999, "New Combustion Concept for Ultra-Clean and High-Efficiency Small DI Diesel Engines", SAE paper 1999-01-3681

[2] Kimura, S., Aoki, O., Kitahara, Y., Aiyoshizawa, E., 2001, "Ultra-Clean Combustion Technology Combining a Low-Temperature and Premixed Combustion Concept for Meeting Future Emission Standards", SAE paper 2001-01-0200

[3] Kimura, S., Ogawa, H., Matsui, Y., Enomoto, Y., 2002, "An Experimental Analysis of Low Temperature and Premixed Combustion for Simultaneous Reduction of NOx and Particulate Emissions in Direct Injection Diesel Engines", International J. of Engine Research, 3(4), pp.249-259

[4] Miles, P. C., Choi, D., Pickett, L.M., Singh, I.P., Henein, N., Rempel Ewert, B.H., Yun, H., Reitz, R.D., 2004, "Rate-Limiting Processes in Late-Injection, Low-Temperature Diesel Combustion Regimes", Thiesel Conference 2004, Valencia (Spain)

[5] Choi, D., Miles, P.C.; Yun, H., Reitz, R.D., 2004, "A parametric study of low-temperature, late-injection combustion in a HSDI diesel engine", 6th International Symposium on Diagnostics and Modeling of Combustion in Internal Combustion Engines (COMODIA); August 2-5; Yokohama, JAPAN

[6] Yanagihara, H., 2002, "A Study on Combustion Structure of Premixed Compression Ignition Diesel Engines", SAE paper 2002-30-0009

[7] Musculus, M.P.B., 2004, "On the Correlation between NOx Emissions and the Diesel Premixed Burn", SAE paper 2004-01-1401

[8] Dec, J.E., 1997, "A conceptual Model of D.I. Diesel Combustion Based on Lased Sheet Imaging", SAE Paper 970873

[9] Singh, S., Reitz, R.D., Musculus, M.P.B., 2005, "2-colors Thermometry Experiments and High-Speed Imaging of Multimode Diesel Engine Combustion", SAE paper 2005-01-3842

[10] Lachaux, T., and Musculus, M. P. B., 2007, "In-Cylinder Unburned Hydrocarbon Visualization During Low-Temperature Compression-Ignition Engine Combustion Using Formaldehyde PLIF", Proc.Combust.Inst.31th,pp.2921-2929

[11] Espey, C., and Dec, J. E., 1993, "Diesel Engine Combustion Studies in a Newly Designed Optical-Access Engine using High-Speed Visualization and 2-D Laser Imaging", SAE Paper 930971

[12] Zhao, H., Ladammatos, N., 1999, *Engine Combustion Instrumentation and Diagnostics*, SAE book, ISBN 0-7680-0665-1

[13] Dec, J.E., Espey, C., 1992, "Soot and fuel distributions in a D.I. diesel engine via 2-D imaging", SAE paper 922307

[14] Hulqvist, A., Christensen, M., Johansson, B., Franke, A., Richter, M., Alden, M., 1999, "A study of the Homogeneous Charge Compression Ignition Combustion Process by Chemiluminescence Imaging", SAE paper 1999-01-3680

[15] Dec, J.E., Espey, C., 1995, "Ignition and Early Soot Formation in a D.I. Diesel Engine using Multiple 2-D Imaging Diagnostics", SAE paper 950456

[16] Dec, J. E., Espey, C., 1998, "Chemiluminescence Imaging of Autoignition in a DI Diesel Engine", SAE paper 982685

[17] Dec, J. E., 1992, “Soot Distribution in a D.I. Diesel Engine using 2-D Imaging of Laser-Induced Incandescence, Elastic Scattering, and Flame Luminosity”, SAE Paper 920115
[18] Dec, J.E., Kelly-Zion, P.L., 2000, “The Effects of Injection Timing and Diluent Addition on Late-Combustion Soot Burnout in a Diesel Engine Based on Simultaneous 2-D Imaging of OH and Soot”, SAE paper 2000-01-0238
[19] Dec, J. E., and Coy, E. B., 1996, “OH Radical Imaging in a DI Diesel Engine and the Structure of Early Diffusion Flame”, SAE paper 960831
[20] Musculus, M.P.B., 2006, “Multiple Simultaneous Optical Diagnostic Imaging of Early-Injection Low-Temperature Combustion in a Heavy-Duty Diesel Engine”, SAE paper 2006-01-0079
[21] Heywood, J.B., 1988, *Internal Combustion Engine Fundamentals*, Mc Graw-Hill, New-York
[22] Desantes, J.M., Payri, R., Salvador, F.J., Gimeno J., 2006, “Prediction of Spray Penetration by Means of Spray Momentum Flux”, SAE paper 2006-01-1387
[23] Espey, C., Dec, J. E., 1995, “The Effect of TDC Temperature and Density on the Liquid-Phase Penetration in a D.I. Diesel Engine, SAE paper 952456
[24] Canaan, R.E., Dec, J.E. and Green, R.M., 1998, “The Influence of Fuel Volatility on the Liquid-Phase Fuel Penetration in a Heavy-Duty D.I. Diesel Engine”, SAE paper 980510
[25] Siebers, D.L., 1999, “Scaling Liquid-Phase Fuel Penetration in Diesel Sprays Based on Mixing-Limited Vaporization”, SAE paper 1999-01-0528
[26] Hotta, Y., Nakakita, K., Inayoshi, M., Ogawa, T., Sato, T., Yamada, M., 1998, “Combustion Improvement for Reducing Exhaust Emissions in IDI Diesel Engine”, SAE paper 980503
[27] Tsurushima, T., Zhang, L., Ishii, Y., 1999, “A Study of Unburnt Hydrocarbon Emission in Small DI Diesel Engines”, SAE paper 1999-01-0512
[28] Pickett, L.M., Siebers, D.L., Idicheria, C.A., 2005, “Relationship Between Ignition Processes and the Lift-Off Length of Diesel Fuel Jets”, SAE paper 2005-01-3843
[29] Pickett, L.M., Siebers D.L., 2003, “Fuel effects on soot processes of fuel jets at DI diesel conditions”, SAE paper 2003-01-3080
[30] Mueller, C.J., Pitz, W.J., Pickett, L.M., Martin, G.C., Siebers, D.L., Westbrook, C.K., 2003, “Effects of Oxygenates on Soot Processes in DI Diesel Engines: Experiments and Numerical Simulations”, SAE paper 2003-01-1791
[31] Hasegawa, R., Sakata, I., Koyama, T., Yanagihara, H., 2003, “Numerical Analysis of Ignition Control in HCCI Engine”, SAE paper 2003-01-1817
[32] Kee, R. J., Rupley, F. M., Meeks, E., Miller, J. A., 1996, “A FORTRAN Chemical Kinetics Package for the Analysis of Gas Phase Chemical and Plasma Kinetics”, Sandia National Laboratories, 1996
[33] Lutz, A. E., Kee, R. J., Miller, J. A., 1988, “SENKIN: A FORTRAN Program for Predicting Homogeneous Gas Phase Chemical Kinetics with Sensitivity Analysis”, Sandia National Laboratories, Report SAND87-8248,1988
[34] Ladommatos, N., Suhair, M. A., Zhao, H., Hu, Z., 1998, “Effects of EGR on Heat Release in Diesel Combustion”, SAE paper 980184
[35] Pickett, L. M., Caton, J. A., Musculus, M. P. B., Lutz, A. E., 2006, “Evaluation of the equivalence ratio–temperature region of diesel soot precursor formation using a two-stage Lagrangian model”, International J. of Engine Research, 7(5), pp.349-370
[36] Idicheria, C. A., Pickett, L. M., 2005, “Soot Formation in Diesel Combustion under High-EGR Conditions”, SAE paper 2005-01-3834

Figure Captions

FIGURE 1. Engine cross-section schematic and optical diagnostics set-up and field of view from the piston window (inset).

FIGURE 2. Mass rate of injection and apparent heat release rate. The boxed numbers 1, 2 and 3 represent the cool-flame phase, the premixed-combustion phase, and the mixing-controlled phase, respectively.

FIGURE 3: Liquid-phase (LMS, blue) and vapor-phase (BB-PLIF, green) fuel. The crankshaft angle is displayed on the top left corner and the LMS and BB-PLIF gains are on the bottom of each image. The small white dot marks the injector location and the thick white line indicates the location of bowl-rim, 50 mm from the injector.

FIGURE 4. Liquid length extracted from the liquid Mie scattering (LMS) instantaneous images.

FIGURE 5. Chemiluminescence averaged pictures. The crank angle is displayed on the top left corner while the relative gain is displayed at the bottom left corner. The small white dot marks the injector location and the thick white line indicates the location of bowl-rim, 50 mm from the injector.

FIGURE 6. Natural luminosity intensity, plotted (a) along the jet centerline, and (b) averaged along the centerline.

FIGURE 7. Instantaneous images from fuel and OH fluorescence (green) and laser induced incandescence (red). The crank angle is displayed at the top left corner of the picture while the relative gains are displayed at the bottom. The small white dot marks the injector location and the thick white line indicates the location of bowl-rim, 50 mm from the injector. The vertical dashed line indicates the approximate separation of fluorescence from OH, on the right, and broadband sources (*e.g.*, fuel), on the left.

FIGURE 8. On-line (red) and off-line (green) ensemble averaged OH-PLIF images. The crank angle is displayed on the top left corner while the relative gains are displayed on the bottom. The small white dot marks the injector location and the thick white line indicates the location of bowl-rim, 50 mm from the injector.

FIGURE 9. Instantaneous images of simultaneous OH fluorescence (green) and chemiluminescence and/or soot luminosity (red). Annotation is same as for Fig. 7

Table Captions

TABLE 1: Engine specifications, injector specifications and operating conditions